From Hollow Nanosphere to Hollow Microsphere: Mild Buffer Provides Easy Access to Tunable Silica Structure

Jian Liu,[†,‡] Fengtao Fan,[†,‡] Zhaochi Feng,[†] Lei Zhang,[†] Shiyang Bai,[†,‡] Qihua Yang,*[,†] and Can Li*[,†]

State Key Laboratory of Catalysis, Dalian Institute of Chemical Physics, Chinese Academy of Sciences, 457 Zhongshan Road, Dalian 116023, China, and Graduate School of the Chinese Academy of Sciences, Beijing 100039, China

Received: May 11, 2008; Revised Manuscript Received: August 18, 2008

A facile synthesis method for producing silica hollow spheres from nano- to microsize level is realized by adjusting the hydrolysis and condensation kinetics of silane precursors in a mild buffer solution ($NaH_2PO_4-Na_2HPO_4$, pH $\approx$ 7.0) in the presence of F127 ($EO_{106}PO_{70}EO_{106}$) surfactant. Characterization using transmission electron microscopy, field-emission scanning electron microscopy, and nitrogen sorption techniques reveals that the silica hollow nanospheres with outer diameter of about 12 nm can be obtained with tetramethoxysilane as silane precursor. Silica hollow nanospheres ($\sim$20 nm) can also be prepared using tetraethoxysilane (TEOS) as silane precursor with the addition of hydrolysis and condensation catalyst NH_4F. Using TEOS as the silane precursor without F^-, the formation of silica hollow microspheres (0.5$\sim$8 μm) was observed. Time-resolved in situ UV-Raman results show that TEOS does not hydrolyze at room temperature, and the hydrolysis of TEOS occurs immediately at room temperature when NH_4F was added to the buffer solution. The fast hydrolysis and condensation rates of silane precursor favor the formation of hollow nanospheres through the condensation of silicate around a single micelle of F127 in $NaH_2PO_4-Na_2HPO_4$ buffer solution. The construction of hollow microspheres is attributed to the formation of O/W emulsion by the hydrophobic TEOS with the aid of F127 surfactant due to the existence of unhydrolyzed TEOS at room temperature under current synthetic conditions.

1. Introduction

Hollow structured micro- or nanoscopic spheres have attracted intense research interests in recent years, owing to their unique chemicophysical properties including good permeability, thermal and mechanical stability, low density, high specific surface area, and special optical/electric/magnetic properties.[1−5] Among them, the silica hollow spheres with tunable particle size are of great interest for a number of purposes, for example, in therapeutic, storage, and catalytic applications.

The methods for the synthesis of silica hollow spheres could be roughly classified into sacrificial core methods and interfacial synthesis methods, depending on whether the core material is a solid or a liquid. Polymer latexes,[4,5] inorganic spheres,[6] oil droplets,[3,7−15] vesicle,[16−19] and surfactants micelles[20−23] have been used as the core materials. Some special technologies—such as sonochemical treatment[24] and electrically forced liquid jets[25]—can also be used for the synthesis of silica hollow spheres. Generally, the synthesis of silica hollow spheres with relatively large diameters ranging from submicrometer to micrometer can be accomplished through a number of methods such as emulsion templating,[3,7−15] layer-by-layer (LbL) self-assembly,[4] latexes templating,[5,6] or vesicle templating.[16−19] Polymeric micelles have been demonstrated to be a versatile template for the synthesis of silica hollow spheres with particle size below 100 nm.[20−23] However, in most cases, the products occur as second-order or higher-order aggregates due to the instability of the template micelles under the synthesis conditions.[20] To date, although the reported approaches for the synthesis of silica hollow spheres are quite flexible, these approaches require multiple sequential steps and are not suitable for producing silica hollow nanospheres in large quantities for practical applications.[20] In addition, the generation of silica hollow spheres with size tunable from nano- to micrometer level through a facile synthesis strategy still remains a challenge.

In our previous work, we focused on the synthesis of silica-based hollow spheres, mesoporous silicas, and organosilicas under a mild buffer condition.[7,22,26] We have demonstrated that the organic−inorganic hybrid hollow nanospheres with controllable size and shell thickness can be synthesized using 1,2-bis(trimethoxysilyl)ethane (BTME) as the silane precursor under a mild buffer condition ($NaH_2PO_4-Na_2HPO_4$, pH $\approx$ 7.0).[22] The single F127 micelles stabilized by inorganic electrolytes ($NaH_2PO_4-Na_2HPO_4$) play a main role in the formation of the hollow nanospheres. Under neutral condition, the hydrolysis and condensation rates of the silane precursor will be greatly suppressed. The unhydrolyzed silane precursor such as tetraethoxysilane (TEOS) can form an emulsion with the aid of surfactant, as we and other groups demonstrated previously.[12,13,26,27] The existence of an O/W emulsion can generally lead to the formation of hollow microspheres and adjustment of the mesostructure of the porous materials through altering the phase behavior of the polymer surfactant. Under neutral buffer solution, the facile synthesis of silica hollow nanospheres and microspheres may be realized due to the fact that the behavior of polymer surfactant could be controlled by adding the inorganic electrolyte and by adjusting the hydrolysis and condensation kinetics of the silane precursor.

* To whom correspondence should be addressed. E-mail: yangqh@dicp.ac.cn (Q.Y.), canli@dicp.ac.cn (C.L.); phone: 86-411-84379552; 86-411-84379070; fax: 86-411-84694447; URL: http://www.hmm.dicp.ac.cn, http://www.canli.dicp.ac.cn.

† Dalian Institute of Chemical Physics, Chinese Academy of Sciences.

‡ Graduate School of the Chinese Academy of Sciences.

10.1021/jp804161f CCC: $40.75
Published on Web 09/27/2008

In the present study, we reported the facile synthesis of silica hollow spheres from nano- to microsize level by controlling the behavior of polymer surfactant F127 through adjusting the hydrolysis and condensation kinetics of the silane precursor in a mild buffer solution ($NaH_2PO_4-Na_2HPO_4$, pH $\approx$ 7.0). In situ UV-Raman spectroscopy and dynamic light scattering (DLS) were used to follow the hydrolysis and condensation process of silane precursors. The characterization results show that the discrete silica hollow nanospheres in large quantities can be formed by the condensation of the silane precursors (tetramethoxysilane (TMOS), or TEOS plus NH_4F) with fast hydrolysis and condensation rates around single surfactant micelles. The formation of oil-in-water emulsion by hydrophobic silane precursor with slow hydrolysis and condensation rates leads to the construction of silica hollow microspheres. Under neutral buffer solution ($NaH_2PO_4-Na_2HPO_4$, pH $\approx$ 7.0), the facile synthesis of silica hollow nanospheres and microspheres was realized.

2. Experimental Section

2.1. Chemicals and Reagents. All materials were of analytical grade and were used without any further purification. Triblock poly(ethylene oxide)−poly(propylene oxide)−poly(ethylene oxide) copolymer Pluronic F127 (M_W = 12600, $EO_{106}PO_{70}EO_{106}$) was purchased from Sigma-Aldrich Company Ltd. (U.S.A.). TEOS, TMOS, and other reagents were obtained from Shanghai Chemical Reagent. Inc., of Chinese Medicine Group.

2.2. Synthesis Procedure. ***2.2.1. Synthesis of Silica Hollow Nanospheres (SHN) in $NaH_2PO_4-Na_2HPO_4$ (pH $\approx$ 7.0) Buffer Solution.*** In a typical synthesis, 0.8 g of F127 was dissolved in 28 mL of 40 mM sodium phosphate buffer solution (pH $\approx$ 7.0, 0.020 mol/L NaH_2PO_4, 0.020 mol/L Na_2HPO_4) at 20 °C under vigorous stirring. When the copolymer was dissolved, 3.04 g (20 mmol) of TMOS was added under stirring. The molar composition of the mixture was Si/F127/NaH_2PO_4/Na_2HPO_4/H_2O = 10 000:32:280:280:778 000. The resultant mixture was stirred at 20 °C for 24 h and aged at 100 °C under static conditions for an additional 24 h. The solid product was recovered by filtration and dried under air at room temperature overnight. Finally, the surfactant was extracted by refluxing 1.0 g of the as-synthesized material in 200 mL of ethanol containing 1.5 g of concentrated aqueous HCl solution for 24 h. The extracted sample is SHN. The synthesis condition for SHN-1 was similar to that of SHN, except that 4.17 g (20 mmol) of TEOS was used as the silane precursor and NH_4F was added before the addition of TEOS (molar ratio NH_4F/TEOS = 5%).

2.2.2. Synthesis of Silica Hollow Microspheres (SHM) in $NaH_2PO_4-Na_2HPO_4$ (pH $\approx$ 7.0) Buffer Solution. The synthesis procedure is similar to SHN, except that TEOS was used as the silane precursor. The molar composition of the mixture was Si/F127/NaH_2PO_4/Na_2HPO_4/H_2O = (2500∼15 000):32:280:280:778 000. The surfactant-free samples were denoted as SHM*n* (*n* = 79, 157, 315, 472), where *n* is the molar ratio of Si/F127. The synthesis of sample SHM315-30 was similar to that of SHM315, except that after the addition of 4.17 g (20 mmol) of TEOS, the resultant mixture was stirred at 20 °C only for 30 min.

2.3. Characterization. Transmission electron microscopy (TEM) was performed using a FEI Tecnai G^2 Spirit at an acceleration voltage of 120 kV. Before examination, the samples were dispersed in anhydrous ethanol and were deposited on a holey carbon film on a Cu grid. Field-emission scanning electron microscopy (FESEM) was undertaken on a FEI Quanta 200F microscope and a HITACHI S-4800 microscope operating at an accelerating voltage of 1−30 kV. The nitrogen sorption experiments were performed at −196 °C on a Micromeritics ASAP 2020 and a Quantachrome Autosorb-1 system. Prior to the measurement, the samples were outgassed at 120 °C for 6 h. The BET (Brunauer−Emmett−Teller) specific surface areas were calculated using the adsorption data in a relative pressure range of P/P_0 = 0.05∼0.25. Pore size distribution curve was calculated from the adsorption branch using BJH (Barrett−Joyner−Halenda) method. The total pore volumes were estimated from the amounts adsorbed at the highest relative pressure (P/P_0) for each sample (P/P_0 = 0.99). The micropore analysis of the different materials was performed at −196 °C on a Quantachrome Autosorb-1 system. The microporosity of the hollow nanosphere was calculated using the HK method. FT-IR spectra were collected with a Nicolet Nexus 470 IR spectrometer with KBr pellet. Dynamic light scattering (DLS) measurements were performed at 20 °C using a Coulter Company N4 plus laser-scattering particle meter (detection range: 3−3000 nm). The reaction solution was collected for analysis at given time intervals using a syringe, and the size of the micelles, colloids, and particles were determined during the time of synthesis by DLS. After DLS measurement, this solution was poured into the reaction system. In situ UV-Raman experiments were carried out in an in situ Raman cell that can be operated under high pressure and temperature as described elsewhere.[28] The cell is designed to simulate the real synthesis condition with a magnetic stirrer on the bottom. UV-Raman spectra were measured with a Jobin−Yvon T64000 triple-stage spectrograph with spectral resolution of 2 cm^{-1}. The laser line at 325 nm of a He−Cd laser was used as an excitation source with an output of 50 mW. The power of the laser at the sample was about 3.0 mW.

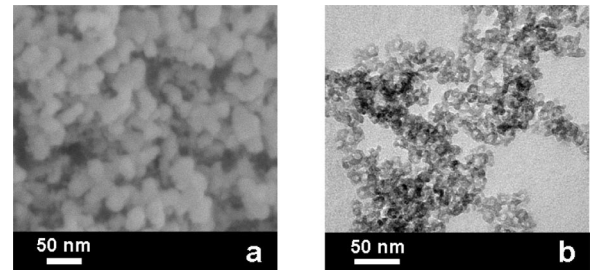

Figure 1. FESEM image (a) and TEM image (b) of SHN (silica hollow nanospheres) synthesized using TMOS as silane precursor in $NaH_2PO_4-Na_2HPO_4$ (pH $\approx$ 7.0) buffer solution.

3. Results and Discussion

The sample silica hollow nanosphere (SHN) was synthesized using TMOS as the silane precursor. The FESEM image of SHN shows the existence of aggregated nanospheres (Figure 1a). The transmission electron microscopy (TEM) image confirms that this sample is composed of hollow nanospheres with an average particle size around 12 nm, a diameter of the hollow interior (void space) of 6 nm, and a shell thickness of 3 nm (Figure 1b). The N_2 adsorption/desorption isotherms exhibit an obvious hysteresis loop at high relative pressure (P/P_0 > 0.85) (Figure 2). The corresponding pore size distribution calculated from the adsorption branch shows pore diameter centered at 5.6 and 28 nm. In addition to the mesoporosity, HK pore size distribution clearly shows that SHN has micropores with diameter in the range of 0.4∼1.0 nm on the shell (Figure 2c). BET surface area and pore volume of SHN are 293 $m^2\ g^{-1}$ and 1.95 $cm^3\ g^{-1}$, respectively (Table 1). The synthesis of silica hollow nanospheres using nonionic Pluronic block copolymer as template

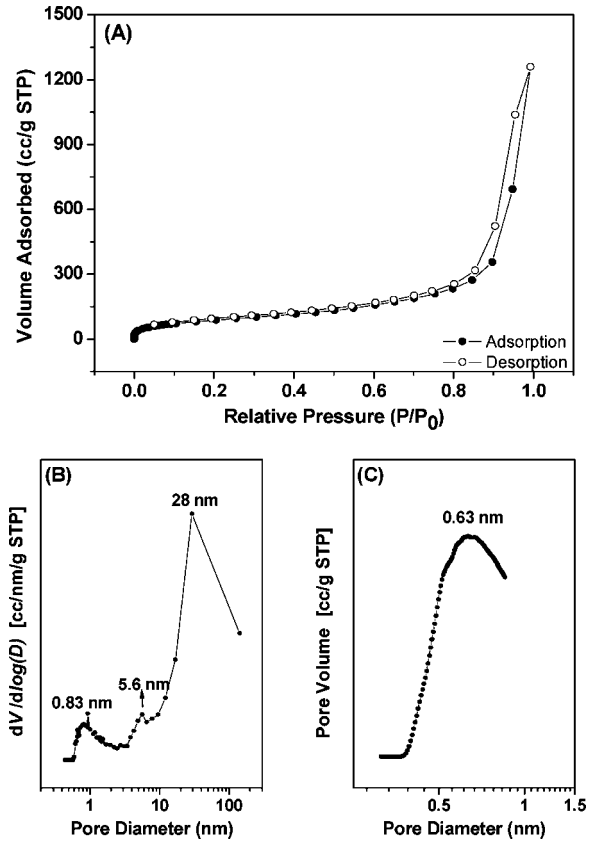

Figure 2. (A) Nitrogen adsorption (●) and desorption (○) isotherm; (B) BJH pore size distribution curve; and (C) HK pore size distribution curve of of SHN synthesized using TMOS as silane precursor in $NaH_2PO_4-Na_2HPO_4$ (pH ≈ 7.0) buffer solution.

TABLE 1: Physicochemical Parameters of the Samples Synthesized at Different Synthetic Conditions

sample	Si/F127 molar ratio	BET specific surface area ($m^2\ g^{-1}$)	micropore volume ($cm^3\ g^{-1}$)	total pore volume ($cm^3\ g^{-1}$)
SHN	315	293	0.12	1.95
SHN-1	315	234	0.10	1.87
SHM315	315	165		0.72
SHM315-30	315	238		0.86
SHM79	79	329		1.27
SHM157	157	210		0.95
SHM472	472	188		0.64

was also reported by Liu and co-workers under strong acidic conditions.[21]

The SHM315 sample was synthesized under conditions similar to SHN but using TEOS as silane precursor. As shown in Figure 3, the hollow microspheres with particle size in the range of 0.5−8 μm and very thin shell were clearly observed in the FESEM images of this sample. From the broken pieces, one can see that the microspheres indeed have a hollow interior. The SHMs have a smooth interior surface and a rough exterior surface covered by aggregated silica nanoparticles with particle size in the range of 20−80 nm (Figures 3a-c). The TEM image reveals that the shell thickness of the hollow microspheres is around 25 nm. In addition, there are mesopores with size around 20 nm on the shell of the hollow spheres, which could be due to the interparticle spaces of the aggregated small nanoparticles (Figure 3d).

The morphology of the sample changed from hollow nanospheres to hollow microspheres when the silane precursor was shifted from TMOS to TEOS. TMOS differs from TEOS in

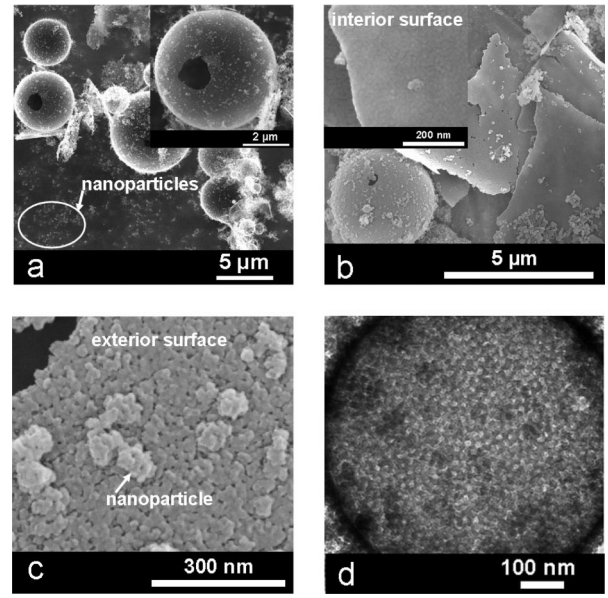

Figure 3. FESEM images (a−c) and TEM image (d) of SHM315 (silica hollow microspheres) synthesized using TEOS as silane precursor in $NaH_2PO_4-Na_2HPO_4$ (pH ≈ 7.0) buffer solution.

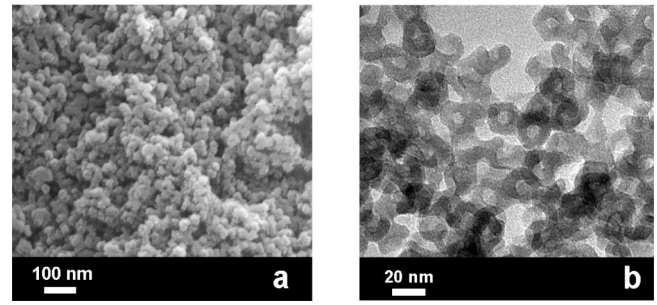

Figure 4. FESEM (a) and TEM (b) images of SHN-1 synthesized using TEOS as silane precursor with the addition of NH_4F in $NaH_2PO_4-Na_2HPO_4$ (pH ≈ 7.0) buffer solution.

the hydrolysis and condensation kinetics and the alcohol species released from the hydrolysis.[29−34] To further understand the reason why the morphology was varied by changing the silane precursor, fluoride was added to accelerate the hydrolysis and condensation rates of TEOS. SHN-1 was synthesized under the conditions similar to SHM315 but with the addition of NH_4F (molar ratio $F^-/Si = 5\%$). Interestingly, the FESEM and TEM images of SHN-1 clearly show that this sample is hollow nanospheres (Figure 4), similar to SHN synthesized using TMOS as precursor. The particle size of the nanospheres was around 20 nm with a hollow interior of about 8 nm and a shell thickness of 6 nm. The N_2 adsorption/desorption isotherms of SHN-1 are type IV with a hysteresis loop at high relatively pressure ($P/P_0 > 0.85$) (Figure 5). The pore size distributions centered at 9.6 and 30 nm were observed in Figure 5b. In addition to the mesoporosity, micropores with diameter in the range of 0.4∼1.0 nm can also be observed in the HK pore size distribution curve. SHN-1 has larger particle size and interior void space but smaller surface area, pore volume, and micropore volume than SHN synthesized using TMOS as precursor (Table 1). FT-IR spectra of the hollow nanospheres before and after extraction are shown in Figure S1 of the Supporting Information. After the extraction step, the intensity of the peaks at 2928 and 2971 cm^{-1} decreased dramatically, and characteristic bands of F127 at 1350, 1459, and 1744 cm^{-1} can hardly be observed, showing that the surfactant is almost completely removed by extraction. The

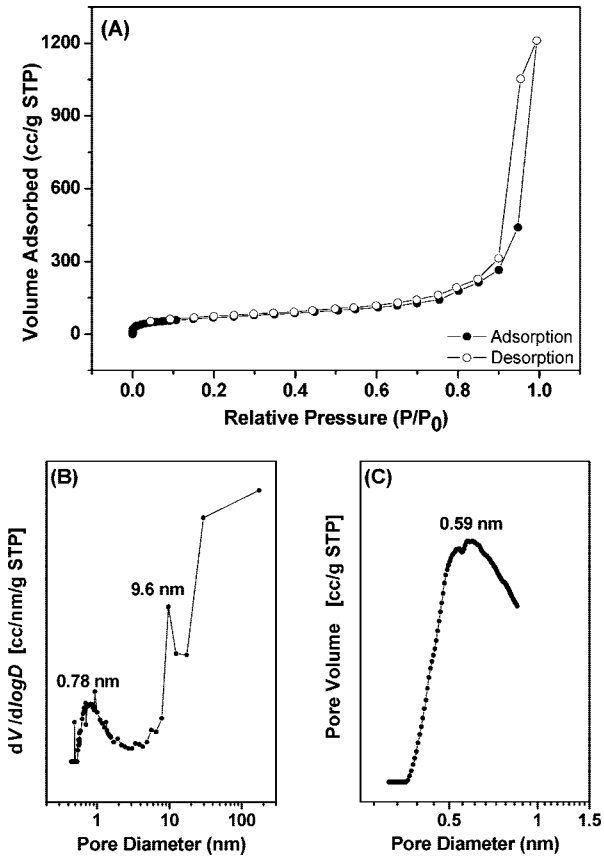

Figure 5. (A) Nitrogen adsorption (●) and desorption (○) isotherm; (B) BJH pore size distribution curve; and (C) HK pore size distribution curve of SHN-1 (silica hollow nanospheres) synthesized using TEOS as silane precursor with addition of NH_4F in $NaH_2PO_4-Na_2HPO_4$ (pH $\approx$ 7.0) buffer solution.

successful surfactant extraction further suggests the existence of micropores on the shell of the hollow nanospheres.

Hydrolysis:

$$\mathrm{Si(OR)_4} + n\mathrm{H_2O} \rightleftharpoons \mathrm{Si(OR)_{4-}}_n\mathrm{(OH)}_n + n\mathrm{ROH} \qquad (1)$$

Condensation:

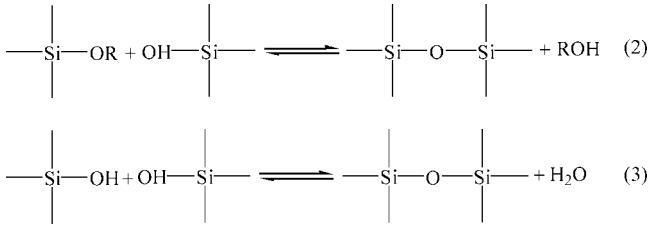

The above results suggest that the morphology of the samples synthesized under current conditions is mainly dependent on the hydrolysis and condensation kinetics of the silane precursors. Raman spectroscopy is a suitable technique to investigate aqueous solutions as well as solid phases of the synthesis mixtures of inorganic materials due to the low Raman scattering cross section of water. Particularly, Raman spectroscopy could be regarded as a powerful tool for the in situ identification of chemical species present in these water and alkoxy silanes mixtures, providing complementary information concerning vibrational spectra of chemical groups.[28,35−37] Hydrolysis and condensation reactions occur when a silicon alkoxide is used to create a sol. Equations 1−3 illustrate the sequence of sol−gel reactions of an alkoxy silane precursor, which consists of reversible hydrolysis (eq 1) and alcohol-producing (eq 2) or water-producing (eq 3) condensation.[36,37] Time-resolved in situ UV-Raman spectroscopy was used to detect the concentration of alcohol and [SiO_4] species and to follow the hydrolysis and condensation kinetics of TEOS and TMOS during the synthetic process (in $NaH_2PO_4-Na_2HPO_4$ buffer solution and in the presence of F127).

The formation of SHM315 using TEOS as precursor was monitored by time-resolved in situ UV-Raman spectroscopy, and the Raman spectra measured before and after hydrothermal treatment are shown in Figure 6. Before hydrothermal treatment, the solution shows similar Raman spectra before and after being stirred for 24 h. Four main peaks, located at 656, 800, 936, and 1090 cm^{-1}, which can be assigned to the SiO_4 (sym), SiO_4 (asym), C−C (sym), and C−O (asym), respectively, stretches of TEOS were observed,[37] and bands related with ethanol (EtOH) can not be observed, indicating that TEOS did not hydrolyze in the buffer solution even after stirring for 24 h (Figure 6A). After hydrothermal treatment, the Raman spectra evolution with time shows the rapid decrease in the peak intensity of TEOS at 656, 800, 936, and 1090 cm^{-1}, and these peaks disappear completely after hydrothermal treatment for 120 min (Figure 6B). After hydrothermal treatment for 60 min, the bands related with EtOH appear at 883 (C−C−O stretch) and 1050 cm^{-1}(C−O sym stretch), which shows the hydrolysis of TEOS. The intensity of these peaks increases with extending hydrothermal treatment time. Raman results show that TEOS did not hydrolyze in $NaH_2PO_4-Na_2HPO_4$ buffer solution without hydrothermal treatment. The hydrophobic TEOS under the synthetic conditions can form oil-in-water emulsion with the aid of F127 surfactant.[12−15,26,27,34] The hydrolysis and condensation of TEOS can only start after hydrothermal treatment. With the hydrothermal treatment, TEOS in the emulsion can diffuse to the interface of the O/W emulsion to condense, which leads to the formation of the SHM. At the same time, the TEOS that did not participate in the formation of emulsion can also condense, thus resulting in the formation of the small silica nanoparticles. The small silica nanoparticles may prefer adhering to large silica hollow particles due to chemical bonds, the electrostatic interaction or attractive London-van der Waals force, and the increase in entropy.[16,31] As a result, a mixture of small nanoparticles and hollow microspheres coated with small nanoparticles on the surface was obtained.

The time-resolved in situ UV-Raman spectra of the synthesis process of SHN-1 (synthesized using TEOS as precursor with the addition of NH_4F) are shown in Figure 7. In the first 10 min of stirring, the dominant peaks in the UV-Raman spectrum are from TEOS at 656, 800, 936, and 1090 cm^{-1}. The weak peak at 883 cm^{-1} from EtOH appears after 10 min of stirring, showing that the hydrolysis of TEOS starts. Compared with the above results, the addition of NH_4F greatly accelerates the hydrolysis rate of TEOS. As the stirring time prolongs, the bands of EtOH at 883 and 1050 cm^{-1} become more visible, accompanied with the decreasing of intensity of the bands associated with TEOS at 656, 800, and 936 cm^{-1}. After 290 min, the peaks at 656, 800, 936, and 1090 cm^{-1}, which are assigned to TEOS, are not present. These spectra undoubtedly show that the concentration of TEOS decreases and is accompanied with the generation of EtOH. TEOS completely hydrolyzed after 5 h of stirring at 20 °C in the presence of NH_4F. Recently, we found that the organic−inorganic hollow nanospheres could be also formed under similar conditions using

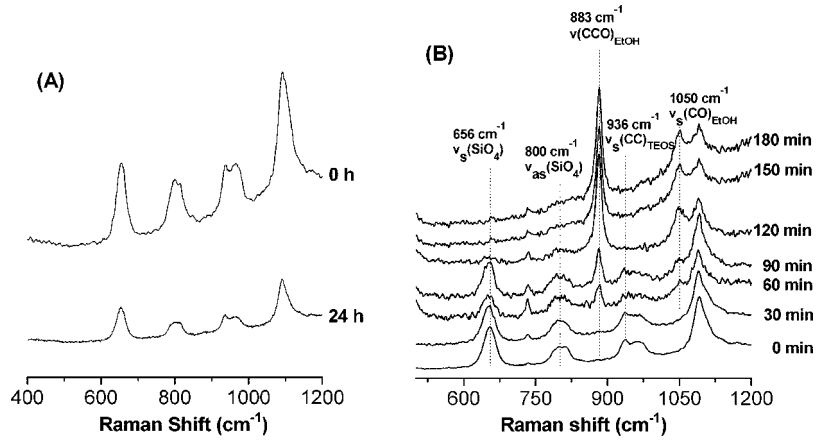

Figure 6. Time-resolved in situ Raman spectra monitoring the hydrolysis of TEOS during the synthesis process of SHM315 (synthesized using TEOS as silane precursor in $NaH_2PO_4-Na_2HPO_4$ (pH ≈ 7.0) buffer solution) (A) before hydrothermal treatment and (B) during hydrothermal treatment at 100 °C.

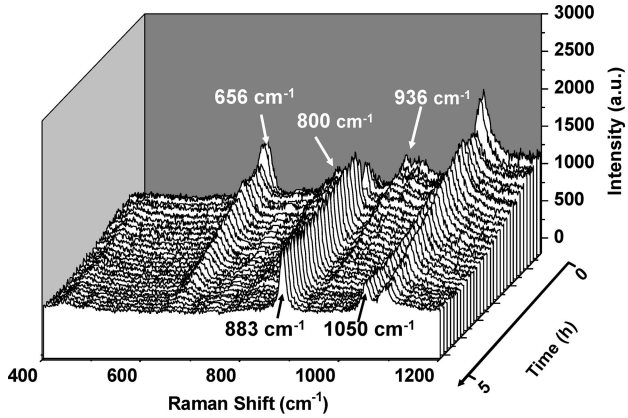

Figure 7. Time-resolved in situ Raman spectra monitoring the hydrolysis process of TEOS during the synthesis of SHN-1 at 20 °C (using TEOS as silane precursor with the addition of NH_4F in $NaH_2PO_4-Na_2HPO_4$ (pH ≈ 7.0) buffer solution after addition of TEOS).

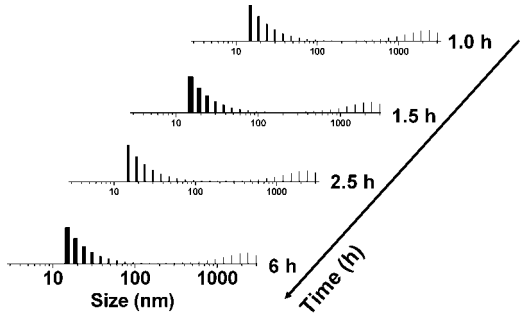

Figure 8. Time-resolved dynamic light scattering (DLS) monitoring the hydrodynamic diameters of the particles during the synthesis of SHN-1 at 20 °C (using TEOS as silane precursor with the addition of NH_4F in $NaH_2PO_4-Na_2HPO_4$ (pH ≈ 7.0) buffer solution after addition of TEOS).

1,2-bis(trimethoxysilyl)ethane (BTME) as silane precursor.[22] Our studies showed that the surfactant (F127) exists as individual micelles at low buffer concentration (20 to 100 mM). The in situ UV-Raman spectrum of the synthesis process of SHN (synthesized using TMOS as precursor) after 2 min stirring shows only one peak at 1020 cm^{-1}, assigned to methanol (MeOH) (C−O sym stretch) (see Figure S2 of the Supporting Information), indicating that TMOS can completely hydrolyze under the current synthetic conditions after several minutes of stirring. When TMOS was used as silane precursor, the hollow

TABLE 2: Time-resolved DLS Monitoring of the Hydrodynamic Diameters of the Particles during the Synthesis of SHM315[a] Before Hydrothermal Treatment

reaction time (h)	hydrodynamic diameters of the particles
1.5	>3 μm
2.5	>3 μm
6	>3 μm

[a] Synthesized using TEOS as silane precursor in $NaH_2PO_4-Na_2HPO_4$ (pH ≈ 7.0) buffer solution.

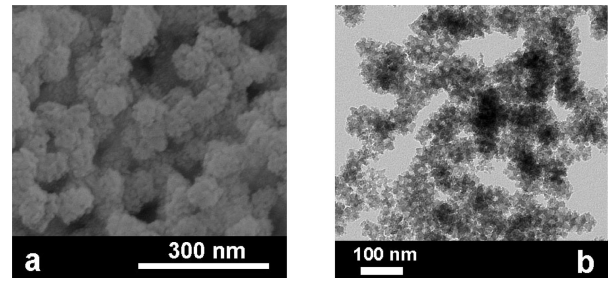

Figure 9. FESEM image (a) and TEM image (b) of SHM315-30 synthesized using TEOS as silane precursor with stirring time of 30 min in $NaH_2PO_4-Na_2HPO_4$ (pH ≈ 7.0) buffer solution.

nanospheres could be formed by condensation of silicate species around the single F127 micelle (with F127 concentration of 2.78 wt %). The results of time-resolved in situ UV-Raman clarify that the hydrolysis rate decreases in the order of TMOS > TEOS + NH_4F > TEOS under $NaH_2PO_4-Na_2HPO_4$ buffer solution. The faster hydrolysis rate of silane precursor leads to the formation of SHN, and the slower hydrolysis rate of the silane precursor favors of the formation of SHM.

To gain a deeper insight into the formation mechanism of the hollow spheres, the evolution of particle size with reaction time was determined with DLS technique. The time-resolved DLS histograms of the synthesis process of SHN-1 (synthesized using TEOS as precursor with the addition of NH_4F) are shown in Figure 8. The average hydrodynamic diameter of F127 micelle in 40 mM buffer solution was 15∼24 nm, as we reported previously.[22] The DLS histograms remain almost the same during the reaction time from 1 to 6 h. Two main particle size distributions were observed in the range of 15∼120 nm and in the range of 0.3∼2.5 μm. Combined with the results of TEM and in situ UV-Raman spectra, we can deduce that these particle size distributions are mainly due to the hollow nanospheres and

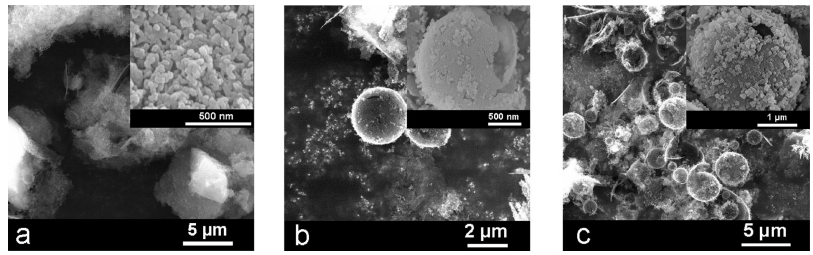

Figure 10. FESEM images of SHM*n* (n = 79, 157, 472) synthesized using TEOS as silane precursor in $NaH_2PO_4-Na_2HPO_4$ buffer solution (pH ≈ 7.0) with different TEOS/F127 molar ratio (a) SHM79, (b) SHM157, and (c) SHM472.

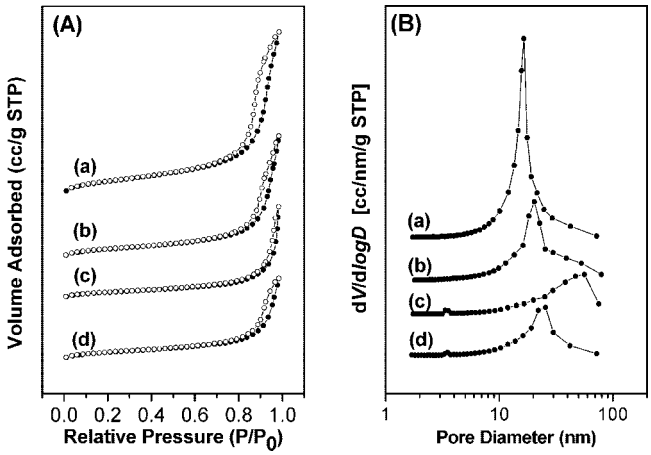

Figure 11. Nitrogen adsorption (●) and desorption (○) isotherm curves (A) and the corresponding pore size distribution (B) of SHM*n* (n = 79, 157, 315, 472) synthesized using TEOS as silane precursor in $NaH_2PO_4-Na_2HPO_4$ buffer solution (pH ≈ 7.0) with different TEOS/F127 molar ratio (a) SHM79; (b) SHM157; (c) SHM315; (d) SHM472.

the aggregated hollow nanospheres. The results of time-resolved DLS analysis of SHM315 (synthesized using TEOS as precursor without F^-) are summarized in Table 2. At room temperature, the mean dynamic diameter larger than 3 μm was observed, which is due to the emulsion droplets formed by F127 surfactant and unhydrolyzed TEOS. The DLS results further confirm the formation of O/W emulsion during the synthesis of SHM315.

The above results suggest that SHMs were obtained using TEOS as silane precursor because of the formation of O/W emulsion by unhydrolyzed TEOS. For further confirming the proposed formation mechanism, the effects of the stirring time[3,8,10] and the TEOS concentration on the morphology of the samples were investigated. Figure 9 shows the FESEM and TEM images of SHM315-30 prepared using TEOS as precursor with a stirring time of 30 min. Strawberry-like particles (particle size of 80 nm) composed of nanoparticles (~15 nm) are scattered in the FESEM image of SHM315-30 (Figure 9a). No hollow microspheres could be observed. The TEM image of this sample clearly shows the formation of the nanoparticle aggregates (Figure 9b). Compared with stirring time of 24 h for sample SHM315, the short stirring time for SHM315-30 can not lead to the formation of emulsion even if the oil phase presents. This result further confirms that emulsion formation is necessary to obtain SHMs. SHM315-30 exhibits higher BET specific surface area and pore volume than SHM315 (Table 1).

SHM*n* (n = 79, 157, 472) samples were synthesized with different Si/F127 ratio for further confirming the formation of O/W emulsion during the synthesis process of SHM315. The FESEM images of SHM*n* (n = 79, 157, 472) are displayed in Figure 10. The large agglomerated particles were observed in the SEM image of SHM79. The FESEM image confirms that the large particles were constructed by small nanoparticles with particle size of ~40 nm. When the molar ratio of Si/F127 was increased to 157, the hollow microspheres (1~3 μm) with nanoparticles on the shell were scattered among the nanoparticles. The hollow microspheres have smooth interiors and rough exteriors similar to SHM315. SHM315 synthesized at a Si/F127 molar ratio of 315 is mainly composed of hollow microspheres with nanoparticles distributed uniformly on the shell as mentioned above (Figure 3). SHM472 was a hollow microsphere similar to SHM315 except that more silica nanoparticles deposited on the shell. By varying the molar ratio of Si/F127 from 79:1 to 472:1, the morphologies of the samples change from agglomerated particles to hollow microspheres. At low TEOS concentration, the O/W emulsion can not be formed. The TEOS will hydrolyze and condense around the single F127 micelle. Due to the slow hydrolysis and condensation rate, TEOS can not solidify with fast speed at the interaction phase of the single micelle. Thus, only silica nanoparticles were formed. At higher concentration of TEOS, the amount of TEOS is enough for the formation of O/W emulsion with F127 surfactant. TEOS will diffuse to the interface of O/W emulsion and condense, leading to SHMs. Simultaneously, the nanoparticles were also produced as we mentioned above. The N_2 adsorption/desorption isotherms of these samples (SHM79, SHM157, SHM315, and SHM472) exhibit an obvious hysteresis loop over a wide range of relative pressures (Figure 11). With increasing Si/F127 molar ratio from 79 to 472, the BET specific surface areas gradually decrease from 329 to 165 $m^2\ g^{-1}$, accompanied with a decrease of pore volume from 1.27 to 0.64 $cm^3\ g^{-1}$ (Table 1).

4. Conclusions

A facile method has been developed for the synthesis of silica hollow spheres from nano- to microsize level under $NaH_2PO_4-Na_2HPO_4$ (pH ≈ 7.0) buffer solution. The hollow nanospheres can be obtained by using TMOS as a precursor or by using TEOS as a precursor with the addition of NH_4F. The hollow microspheres can also be prepared under similar conditions with TEOS as a precursor without the addition of NH_4F. The results of the time-resolved in situ UV-Raman spectroscopy show that the hydrolysis rate of silane precursors decreases in the order of TMOS > TEOS + NH_4F > TEOS. Hollow nanospheres were obtained using silane precursor with fast hydrolysis rate. Hollow microspheres were formed using silane precursor with a slow hydrolysis rate, which hydrolyzed only after a hydrothermal treatment. The unhydrolyzed and hydrophobic TEOS can form an O/W emulsion with the aid of F127 surfactant, which contributes to the construction of the hollow microspheres. The silica hollow spheres from nano- to microsize levels present potential uses in microencapsulation as well as catalytic applications.

Acknowledgment. This work was supported by the National Natural Science Foundation of China (20503028, 20673113)

and National Basic Research Program of China (2003CB615803, 2005CB221407). We thank Aiping Jia and Professor Mengfei Luo for FESEM characterization.

Supporting Information Available: FT-IR spectra of as-synthesized and extracted hollow nanospheres, and in situ Raman spectrum of SHN. This information is available free of charge via the Internet at http: //pubs.acs.org.

References and Notes

(1) (a) Sun, Q.; Vrieling, E. G.; van Santen, R. A.; Sommerdijk, N. A. J. M. *Curr. Opin. Solid State Mater. Sci.* **2004**, *8*, 111–120. (b) Caruso, F. *Adv. Mater.* **2001**, *13*, 11–22. (c) Caruso, F. *Chem.—Eur. J.* **2000**, *6*, 413–419.

(2) Dinsmore, A. D.; Hsu, M. F.; Nikolaides, M. G.; Marques, M.; Bausch, A. R.; Weitz, D. A. *Science* **2002**, *298*, 1006–1009.

(3) Schacht, S.; Huo, Q. S.; Voigt-Martin, I. G.; Stucky, G. D.; Schüth, F. *Science* **1996**, *273*, 768–771.

(4) (a) Caruso, F.; Caruso, R. A.; Möhwald, H. *Science* **1998**, *282*, 1111–1114. (b) Zelikin, A. N.; Becker, A. L.; Johnston, A. P. R.; Wark, K. L.; Turatti, F.; Caruso, F. *ACS Nano* **2007**, *1*, 63–69. (c) Johnston, A. P. R.; Cortez, C.; Angelatos, A. S.; Caruso, F. *Curr. Opin. Colloid Interface Sci.* **2006**, *11*, 203–209.

(5) Darbandi, M.; Thomann, R.; Nann, T. *Chem. Mater.* **2007**, *19*, 1700–1703.

(6) Chen, J.-F.; Ding, H.-M.; Wang, J.-X.; Shao, L. *Biomaterials* **2004**, *25*, 723–727.

(7) Liu, J.; Li, C. M.; Yang, Q. H.; Yang, J.; Li, C. *Langmuir* **2007**, *23*, 7255–7262.

(8) (a) Sun, Q.; Kooyman, P. J.; Grossmann, J. G.; Bomans, P. H. H.; Frederik, P. M.; Magusin, P. C. M. M.; Beelen, T. P. M.; van Santen, R. A.; Sommerdijk, N. A. J. M. *Adv. Mater.* **2003**, *15*, 1097–1100. (b) Sun, Q.; Magusin, P. C. M. M.; Mezari, B.; Panine, P.; van Santen, R. A.; Sommerdijk, N. A. J. M. *J. Mater. Chem.* **2005**, *15*, 256–259. (c) Botterhuis, N. E.; Sun, Q.; Magusin, P. C. M. M.; van Santen, R. A.; Sommerdijk, N. A. J. M. *Chem.—Eur. J.* **2006**, *12*, 1448–1456.

(9) Lin, H.; Cui, K.; Yao, Y.; Cai, Q.; Feng, Q.; Li, H. *Chem. Lett.* **2005**, *34*, 918–919.

(10) (a) Fujiwara, M.; Shiokawa, K.; Tanaka, Y.; Nakahara, Y. *Chem. Mater.* **2004**, *16*, 5420–5426. (b) Fujiwara, M.; Shiokawa, K.; Sakakura, I.; Nakahara, Y. *Nano Lett.* **2006**, *6*, 2925–2928.

(11) (a) Yu, C. Z.; Tian, B. Z.; Fan, J.; Stucky, G. D.; Zhao, D. Y. *Chem. Lett.* **2002**, 62–63. (b) Zhou, X. F.; Qiao, S. Z.; Hao, N.; Wang, X. L.; Yu, C. Z.; Wang, L. Z.; Zhao, D. Y.; Lu, G. Q. *Chem. Mater.* **2007**, *19*, 1870–1876.

(12) Zhang, H.; Wu, J.; Zhou, L.; Zhang, D.; Qi, L. *Langmuir* **2007**, *23*, 1107–1113.

(13) Fowler, C. E.; Khushalani, D.; Mann, S. *J. Mater. Chem.* **2001**, *11*, 1968–1971.

(14) Yeh, Y. Q.; Chen, B. C.; Lin, H. P.; Tang, C. Y. *Langmuir* **2006**, *22*, 6–9.

(15) Wang, Q.; Liu, Y.; Yan, H. *Chem. Commun.* **2007**, 2339–2341.

(16) (a) Djojoputro, H.; Zhou, X. F.; Qiao, S. Z.; Wang, L. Z.; Yu, C. Z.; Lu, G. Q. *J. Am. Chem. Soc.* **2006**, *128*, 6320–6321. (b) Yu, M.; Wang, H. N.; Zhou, X.; Yuan, P.; Yu, C. Z. *J. Am. Chem. Soc.* **2007**, *129*, 14576–14577.

(17) Wang, J.; Xiao, Q.; Zhou, H.; Sun, P.; Yuan, Z.; Li, B.; Ding, D.; Shi, A. C.; Chen, T. *Adv. Mater.* **2006**, *18*, 3284–3288.

(18) Tan, B.; Vyas, S. M.; Lehmler, H.-J.; Knutson, B. L.; Rankin, S. E. *Adv. Funct. Mater.* **2007**, *17*, 2500–2508.

(19) Li, Y.; Shi, J.; Hua, Z.; Chen, H.; Ruan, M.; Yan, D. *Nano Lett.* **2003**, *3*, 609–612.

(20) (a) Yuan, J. J.; Mykhaylyk, O. O.; Ryan, A. J.; Armes, S. P. *J. Am. Chem. Soc.* **2007**, *129*, 1717–1723. (b) Khanal, A.; Inoue, Y.; Yada, M.; Nakashima, K. *J. Am. Chem. Soc.* **2007**, *129*, 1534–1535. (c) Wan, Y.; Yu, S. H. *J. Phys. Chem. C* **2008**, *112*, 3641–3647.

(21) Huo, Q. S.; Liu, J.; Wang, L.-Q.; Jiang, Y.; Lambert, T. N.; Fang, E. *J. Am. Chem. Soc.* **2006**, *128*, 6447–6453.

(22) Liu, J.; Yang, Q. H.; Zhang, L.; Yang, H. Q.; Gao, J. S.; Li, C. *Chem. Mater.* **2008**, *20*, 4268–4275.

(23) Tang, J. W.; Zhou, X. F.; Zhao, D. Y.; Lu, G. Q.; Zou, J.; Yu, C. Z. *J. Am. Chem. Soc.* **2007**, *129*, 9044–9048.

(24) (a) Shiomi, T.; Tsunoda, T.; Kawai, A.; Chiku, H.; Mizukami, F.; Sakaguchi, K. *Chem. Commun.* **2005**, 5325–5327. (b) Shiomi, T.; Tsunoda, T.; Kawai, A.; Mizukami, F.; Sakaguchi, K. *Chem. Mater.* **2007**, *19*, 4486–4493. (c) Shiomi, T.; Tsunoda, T.; Kawai, A.; Mizukami, F.; Sakaguchi, K. *Chem. Commun.* **2007**, 4404–4406.

(25) Bruinsma, P. J.; Kim, A. Y.; Liu, J.; Baskaran, S. *Chem. Mater.* **1997**, *9*, 2507–2512.

(26) Liu, J.; Yang, Q. H.; Zhang, L.; Jiang, D. M.; Shi, X.; Yang, J.; Zhong, H.; Li, C. *Adv. Funct. Mater.* **2007**, *17*, 569–576.

(27) Shah, J.; Pinnavaia, T. J. *Chem. Commun.* **2005**, 1598–1600.

(28) Fan, F. T.; Feng, Z. C.; Li, G. N.; Sun, K. J.; Ying, P. L.; Li, C. *Chem.—Eur. J.* **2008**, *14*, 5125–5129.

(29) Bao, X. Y.; Li, X.; Zhao, X. S. *J. Phys. Chem. B* **2006**, *110*, 2656–2661.

(30) (a) Tan, B.; Rankin, S. E. *J. Non-Cryst. Solids* **2006**, *352*, 5453–5462. (b) Tan, B.; Rankin, S. E. *J. Phys. Chem. B* **2006**, *110*, 22353–22364.

(31) Brinker, C. J.; Scherer, G. W. *Sol-Gel Science: The Physics and Chemistry of Sol-Gel Processing*; Academic Press: New York, 1990.

(32) Brinker, C. J. *J. Non-Cryst. Solids* **1988**, *100*, 31–50.

(33) Hook, R. J. *J. Non-Cryst. Solids* **1996**, *195*, 1–15.

(34) Liu, J.; Zhang, L.; Yang, Q. H.; Li, C. Microporous Mesoporous Mater. 2008. in press, DOI: 10.1016/j. micromeso. 2008.04.030.

(35) Tejedor-Tejedor, M. I.; Paredes, L.; Anderson, M. A. *Chem. Mater.* **1998**, *10*, 3410–3421.

(36) (a) Baccile, N.; Teixeira, C. V.; Amenitsch, H.; Villain, F.; Lindén, M.; Babonneau, F. *Chem. Mater.* **2008**, *20*, 1161–1172. (b) Venditti, F.; Angelico, R.; Palazzo, G.; Colafemmina, G.; Ceglie, A.; Lopez, F. *Langmuir* **2007**, *23*, 10063–10068. (c) Marino, I.-G.; Lottici, P. P.; Bersani, D.; Raschellà, R.; Lorenzi, A.; Montenero, A. *J. Non-Cryst. Solids* **2005**, *351*, 495–498.

(37) (a) Artaki, I.; Bradley, M.; Zerda, T. W.; Jonas, J. *J. Phys. Chem.* **1985**, *89*, 4399–4404. (b) Matos, M. C.; Ilharco, L. M.; Almeida, R. M. *J. Non-Cryst. Solids* **1992**, *147−148*, 232–237. (c) Kalyanasundaram, K.; Thomas, J. K *J. Phys. Chem.* **1976**, *80*, 1462–1473.

JP804161F